Physica B 715 (2025) 417515

Contents lists available at ScienceDirect

Physica B: Condensed Matter

journal homepage: www.elsevier.com/locate/physb

Suppression of the Mott insulating phase in the particle-hole asymmetric Hubbard model

Mateus Marques [a], Bruno M. de Souza Melo [b], Alexandre R. Rocha [c], Caio Lewenkopf [b,d], Luis G.G.V. Dias da Silva [a,*]

[a] Instituto de Física, Universidade de São Paulo, Rua do Matão 1371, São Paulo, SP 05508-090, Brazil
[b] Instituto de Física, Universidade Federal Fluminense, Niterói, RJ 24210-346, Brazil
[c] Instituto de Física Teórica, São Paulo State University (UNESP), São Paulo, SP 01140-070, Brazil
[d] Instituto de Física, Universidade Federal do Rio de Janeiro, Rio de Janeiro, RJ 21941-909, Brazil

ARTICLE INFO

Keywords:
DMFT
Hubbard model
Mott transition
Particle-hole symmetry

ABSTRACT

We explore the phase diagram of the Mott metal–insulator transition (MIT), focusing on the effects of particle-hole asymmetry (PHA) in the single-band Hubbard model. Our dynamical mean-field theory (DMFT) study reveals that the introduction of PHA in the model significantly influences the critical temperature (T_c) and interaction strength (U_c), as well as the size of the co-existence region of metallic and insulating phases at low temperatures. Specifically, as the system is moved away from particle-hole symmetry, T_c decreases and U_c increases, indicating a suppression of the insulating phase and the strengthening of the metallic behavior. Additionally, the first-order transition line between metallic and insulating phases is better defined in the model with PHA, leading to a reduced co-existence region at $T < T_c$. Moreover, we propose that the MIT can be characterized by the charge density, which serves as a viable alternative to zero-frequency spectral density typically used in DMFT calculations. Our findings provide new insights into the role of particle-hole asymmetry in the qualitative and quantitative characterization of the MIT even in a very simple system.

1. Introduction

A complete understanding of strong correlations in materials remains one of the greatest challenges in condensed matter physics [1,2]. The competition between itinerant and correlated behavior of the electrons gives rise to rich and complex phenomena with promising applications such as oxide electronics, high-temperature superconductors, and spintronic devices [3–6].

A classical topic in this field is the study of the Mott metal–insulator transition (MIT) [7], occurring when the electron–electron interactions are relatively large, of the order of the bandwidth. In this scenario, the electrons can become localized, leading to an insulating state. On the other hand, as the interactions are reduced and the electrons can become itinerant, the system transitions into a strongly correlated metal phase [8]. In actual experiments, the MIT can be induced by varying temperature, pressure, and composition of the materials in the system [9–11].

One conventional approach to study the qualitative effects of strong correlations is the proposition and solution of model Hamiltonians. These models drastically reduce the number of degrees of freedom of the problem to the relevant ones involved in a given phenomenon. From a theoretical point of view, the Hubbard model [12,13] has been successfully used to describe the main features of Mott insulators, like the transition metal oxide V_2O_3 [11,14].

The MIT has been extensively studied in the literature, mostly using the dynamical mean field theory (DMFT) approach [15,16] in models with particle-hole symmetry (PHS). In this case, it is well established that, below a critical temperature, there is a first-order transition line in the temperature (T) versus interaction (U) phase diagram ending in the critical point (U_c, T_c). For $T < T_c$, the system is metallic for $U < U_{c_1}(T)$ and insulating for $U > U_{c_2}(T)$ with a coexistence region (where one of the phases is thermodynamically stable while the other is only metastable) for values of U between these two values [15,17–21]. The two spinodal lines defined by $U_{c_1}(T)$ and $U_{c_2}(T)$ meet at the critical point (U_c, T_c). For $T > T_c$, the transition becomes a crossover [11,14,22].

Interestingly, most of the DMFT investigations have concentrated on the low-temperature regime ($T < T_c$), while the high-temperature crossover region is the one pertinent to numerous experimental setups [23]. Conversely, for $T > T_c$, different crossover regimes have

* Corresponding author.
E-mail address: luisdias@if.usp.br (L.G.G.V. Dias da Silva).

https://doi.org/10.1016/j.physb.2025.417515
Received 18 February 2025; Received in revised form 15 June 2025; Accepted 19 June 2025
Available online 4 July 2025

been tentatively discerned [15], yet they have not been examined in any significant depth [24].

Although less studied, the particle-hole asymmetric (PHA) Hubbard model is of particular interest since that is the prevalent situation for the band structure [17,25,26] of most materials. Particle-hole asymmetry can be implemented in the Hamiltonian model by including next-nearest neighbor hopping matrix elements at half-filling or by explicitly changing the onsite energy [4,8,14,26–29]. As argued above, although the MIT in the Hubbard model has been extensively studied, most of the studies focus on the particle-hole symmetric (PHS) case as this naturally renders the system to be in half-filling (that corresponds to an occupation number $n = 1$) independently of the interaction strength U. A crucial fact is that the MIT can occur *away from PHS* and this will be marked by $n \to 1$ at the transition [27,29]. In other words, at the insulating side of the MIT, the system will be both particle-hole asymmetric (PHA) *and* at half-filling at the same time.

In this work we revisit this problem by studying the Mott metal–insulator transition (MIT) in the particle-hole asymmetric Hubbard model in the Bethe lattice. While earlier studies have addressed the transition away from PHS at zero [27,30] or very low temperatures [29], here we show that the PHA system has a rich phase diagram at non-zero temperatures. As such, our focus here is on the fate of the co-existence region *away* from PHS at larger temperatures. In fact, our results show that this region is *suppressed* as the system moves away from PHS, a fact which has not been properly documented in previous works.

This behavior is characterized by a lower value of the maximum temperature T_c for which a first-order transition between the metallic and insulating phases takes place. For $T > T_c$, the transition is second-order, such that T_c marks the "end" of the first-order transition line [23]. As such, this critical temperature T_c *decreases* as the system moves away from PHS. Although similar decreases in T_c have been seen in doped [31] and disordered systems [32,33], here we provide a systematic analysis of these effects in a "clean" system in which the on-site energy can be independently varied (say, by an external gate-voltage). As such, our approach can be extended to systems in which the density n is not fixed *a priori* and can vary across the MI transition.

More importantly, in the realistic case of systems away from PHS, we show that the charge density can be a reliable marker of the true MIT transition not only at $T \sim 0$ [29] but also for larger temperatures, introducing the interesting prospect of experimentally characterizing the MIT by the electron (or hole) densities. This allows one to characterize the transition by the charge density n rather than by the zero-frequency spectral density $\rho(0)$, the usual parameter considered in theoretical works.

This paper is organized as follows. In Section 2 we briefly present the model and methods used in this study. In Section 3 we show results for the symmetric and asymmetric Hubbard model focusing in the differences displayed by the two cases with regard to the metal–insulator transition. Finally, in Section 4 we present a summary of our findings and conclusions.

2. Model and methods

The single-band Hubbard model [12] reads

$$\hat{H} = -t \sum_{\langle ij\rangle,\sigma} c^{\dagger}_{i\sigma} c_{j\sigma} + \text{H.c.} + U \sum_{i} n_{i\uparrow} n_{i\downarrow} - \epsilon_d \sum_{i,\sigma} n_{i\sigma} \,, \tag{1}$$

where $c^{\dagger}_{j\sigma}(c_{j\sigma})$ is the creation (annihilation) operator of an electron with spin σ at site j, $n_{j\sigma} = c^{\dagger}_{j\sigma} c_{j\sigma}$ is the occupation number operator, t is the hopping amplitude, and $\langle\cdots\rangle$ means that the sum is restricted to nearest neighbors sites.

Our study focuses on the electronic spectral function $\rho(\omega)$ and on the single-electron density n given by

$$n = \int_{-\infty}^{\infty} f(\omega, T)\rho(\omega) d\omega \,, \tag{2}$$

where $f(\omega, T) = (e^{\omega/k_B T} + 1)^{-1}$ is the Fermi-Dirac function at a temperature T. Hence, our goal is to calculate the local lattice interacting single-particle Green's function.

Given the $\mathbf{k}$-dependent lattice Green's function $G(\mathbf{k}, \omega)$, we use the dynamical mean field theory (DMFT) approach [15,16] to obtain the local single-particle Green's function in momentum space $G_{\text{loc}}(\omega) = \sum_{\mathbf{k}} G(\mathbf{k}, \omega)$ and its spectral function $\rho(\omega) = (-1/\pi)\,\text{Im}\,\{G_{\text{loc}}(\omega)\}$. In essence, DMFT maps a lattice many-body problem with many degrees of freedom into an effective single-impurity problem within a self-consistent cycle. As such, this method addresses the limiting and intermediate regimes of the ratio U/t of the model in a single framework.

For the Hubbard model the effective problem can be treated using the single impurity Anderson model (SIAM) [15,34,35]. The implementation of DMFT for different settings is nicely reviewed in Refs. [15,16,35].

We consider the Hubbard model in a Bethe lattice in the limit of infinite coordination ($z \to \infty$). In this case, the hopping needs to be renormalized as $t = t_*/\sqrt{z}$ for the limit to make physical sense. The non-interacting density of states (DOS) then reads [15,36]

$$\rho_0(\epsilon) = \frac{1}{2\pi t_*^2}\sqrt{4t_*^2 - \epsilon^2}, \quad |\epsilon| < 2t_*, \tag{3}$$

where $D = 2t_*$ is the half-bandwidth of the non-interacting model, which we use as our energy unit.

In the effective impurity approximation [15], the single site electrons are coupled to the non-interacting bath through an energy-dependent hybridization function whose form depends on the lattice effective degrees of freedom. For a Bethe lattice, the hybridization function takes the simple form [15]:

$$\Delta(\omega) = t^2 G_{\text{imp}}(\omega) \,, \tag{4}$$

which is calculated self-consistently from the single-site (impurity) Green's function $G_{\text{imp}}(\omega) = (\omega + \epsilon_d - \Delta(\omega) - \Sigma^I(\omega))^{-1}$ where $\Sigma^I(\omega)$ is the interacting self-energy.

The Green's function is obtained by solving the auxiliary impurity model. Over the last decades, several different impurity solvers have been developed like the iterated perturbation theory (IPT) [37–39], numerical renormalization group (NRG) [40,41], equations of motion (EOM) schemes [42–48], auxiliary-boson approaches [49], including the non-crossing (NCA) [50] and one-crossing (OCA) approximations [51], quantum Monte Carlo (QMC) [52]. For each method, there is a region in the parameter space for which the results are more accurate. NRG, for instance, provides excellent real-frequency spectral data at zero temperature, while EOM and the NCA methods work better at higher temperatures. NCA and EOM, however, have well-known limitations in establishing quantitative estimates for quantities such as the critical temperature T_c as compared to, say, QMC [24]. The computational cost is also an important aspect to be considered as NRG and QMC are computationally much more demanding than the EOM or auxiliary-boson approaches [53].

In this work, we use the non-crossing approximation (NCA) [50,54] as an impurity solver.[1] While NCA has well-documented limitations, like in accurately quantifying the parameters U_{c_1} and U_{c_2} [17], it remains a valuable tool for its low computational cost and ability to incorporate finite temperatures [53]. These features allow us to quickly assess a large range of parameters to get a qualitative insight of the main features and differences between the particle-hole symmetric and asymmetric models [18,55] at $T > 0$.

[1] For the calculations, we used the NCA code from Kristjan Haule available at http://hauleweb.rutgers.edu/tutorials/.

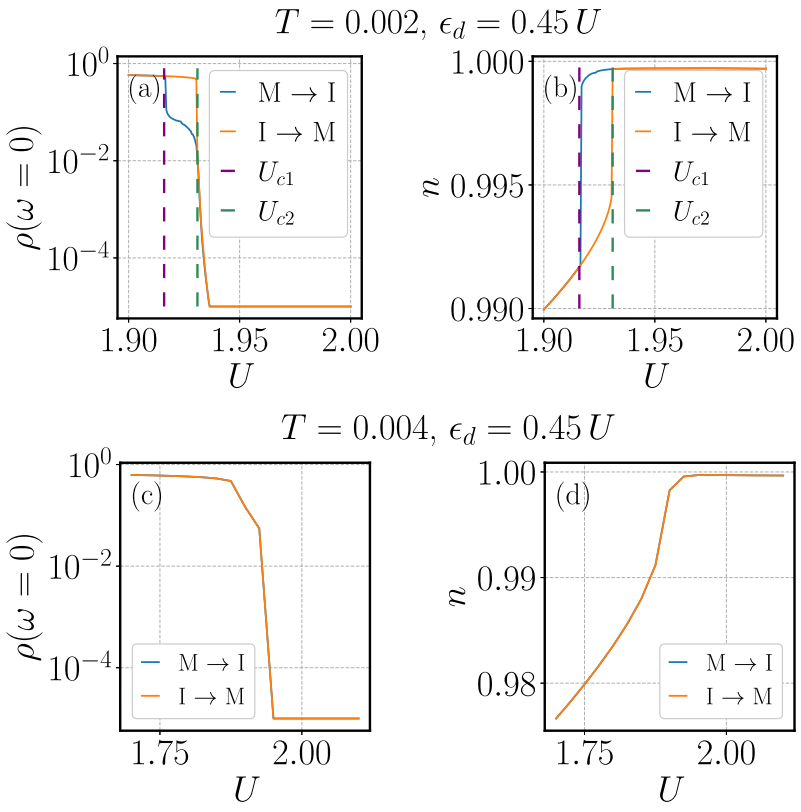

Fig. 1. Occupation n and zero-frequency spectral density $\rho(0)$ versus U for the metal–insulator M → I and the insulator–metal I → M paths for temperatures below and above T_c. Both paths coincide for $T > T_c$.

3. MIT in the hubbard model away from PHS

3.1. Signatures of the MIT from the DMFT results

When the system is away from the particle-hole symmetric point, $\epsilon_d \neq 0.5\,U$, the MIT transition can be characterized by either the occupation n or the zero-frequency spectral density $\rho(0)$ as a function of U. This is illustrated in Fig. 1, which displays n and $\rho(0)$ as a function of U for $\epsilon_d = 0.45\,U$ at two distinct temperatures (below and above T_c).

As it is well-known [15,24], for temperatures lower than a "critical temperature" ($T < T_c$), a co-existence region occurs for $U_{c_1} < U < U_{c_2}$, with first-order transitions occurring at $U = U_{c_1}$ or $U = U_{c_2}$ depending on the path chosen (M → I or I → M, respectively), forming a "hysteresis loop".

These features are clearly identified in the DMFT data shown in Fig. 1 for lower temperatures. At $T = 0.002$, both $\rho(0)$ and n exhibit first-order phase transitions at different values of U, depending on the path taken, as illustrated in Figs. 1(a) and (b). From these results, we can extract the values of U_{c_1} and U_{c_2}, which are marked in the plots. On the other hand, at $T = 0.004$, the co-existence region is negligible and $U_{c_1} = U_{c_2} \equiv U_c$, as shown by Figs. 1(c) and (d).

As a standard procedure, it is useful to define the following quantities:

$$\rho_{\text{avg}}(0) \equiv \left(\rho_{\text{M}\to\text{I}}(0) + \rho_{\text{I}\to\text{M}}(0)\right)/2\,, \qquad (5)$$
$$\Delta\rho(0) \equiv \left|\rho_{\text{I}\to\text{M}}(0) - \rho_{\text{M}\to\text{I}}(0)\right|\,,$$

where $\rho_{\text{M}\to\text{I}}(0)$ and $\rho_{\text{I}\to\text{M}}(0)$ are calculated in the M → I and I → M paths respectively.

From these quantities, we can numerically obtain the transition temperature T_c and the values of U_{c_1} and U_{c_2} by the following method: For each temperature T and path (M → I or I → M), we take the numerical derivative of either $\rho(0)$ or n with respect to U. These derivatives show peaks at the transition points, which correspond to the values of U_{c_1} and U_{c_2}, depending on the path. We can then obtain T_c by identifying the value of T for which these two peaks "merge" (such that $U_{c_1} \approx U_{c_2}$). The numerical error associated with the value of T_c obtained in this way can be reduced by decreasing the discretization steps in both T and U.

3.2. Phase diagrams away from PHS

From these considerations, one can then represent the phase diagram of the system by color plots for $\rho_{\text{avg}}(0)$ as a function of T and U. These are shown in Fig. 2(a)–(d) for different values of the onsite energy ϵ_d. These define T versus U phase diagrams showing the insulating (blue), metallic (red) and co-existence (green) regions. As expected [15,24], the difference between U_{c_2} and U_{c_1} decreases as T increases, such that the co-existence regions narrows to a single point at a critical temperature T_c at which $U_{c_2} = U_{c_1} = U_c$.

Interestingly, the value of T_c (and the overall area of the coexistence region) *decreases* as the system is moved away from the particle-hole symmetric point ($\epsilon_d = 0.5\,U$). This is illustrated in Fig. 2(e), which shows a sharp decrease in T_c as ϵ_d is reduced from $0.5U$ (PHS point) to $0.44U$.[2] In addition, the corresponding value of U_c *increases* as ϵ_d is reduced in the same range, as depicted in Fig. 2(f). In fact, the U_c vs ϵ_d curve is very well approximated by a quadratic scaling of the form $U_c(\epsilon_d) - U_{c0} \sim (\epsilon_d - U/2)^2$ (solid line in Fig. 2(f)), where U_{c0} is the minimal value at the particle-hole symmetry point $\epsilon_d = U/2$. This excellent agreement with a quadratic scaling is consistent with analytical expressions relating U_c and the chemical potential in the context of the doping-driven Mott transition [29,30].

[2] Numerical instabilities in the NCA calculations prevented us from exploring the regime of temperatures lower than $T \sim 0.002$, which restricts our analysis to the range $0.44U \lesssim \epsilon_d \leq 0.5U$.

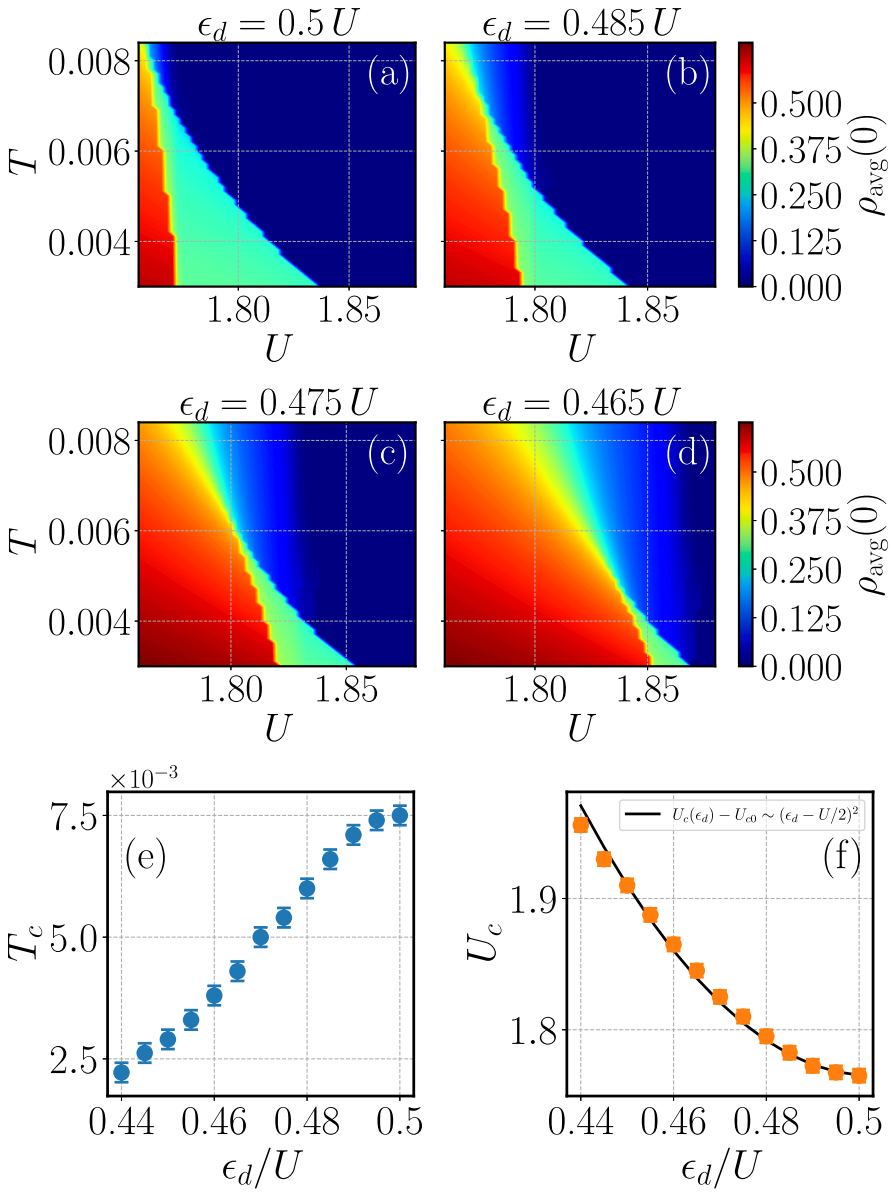

Fig. 2. (a–d) Phase diagrams $U \times T$ for the Hubbard model as it is moved away from particle-hole symmetry: (a) $\epsilon_d = 0.5U$ (PHS) (b) $\epsilon_d = 0.485U$ (c) $\epsilon_d = 0.475U$ (d) $\epsilon_d = 0.465U$. Notice that the co-existence region becomes significantly smaller as the system is moved away from the PHS point. (e–f) T_c and U_c (obtained from the method described in the main text) versus ϵ_d, showing a decrease in T_c and an increase in U_c as ϵ_d is shifted away from the PHS point.

Alternatively, phase diagrams can be visualized by plotting color maps of $\rho_{\rm avg}(0)$ and $\Delta\rho(0)$, defined in Eq. (5), in the $U \times \epsilon_d$ plane for a given temperature T. This is illustrated for $T = 0.002$ in Figs. 3(a) and (b) and for $T = 0.004$ by Figs. 3(c) and (d). We note that both $\rho_{\rm avg}(0)$ and $\Delta\rho(0)$ are symmetric with respect to the PHS value $\epsilon_d = 0.5U$ for all temperatures. Consequently, the curves $U_c(\epsilon_d)$ and $T_c(\epsilon_d)$ shown in Fig. 2 are also symmetric with respect to $\epsilon_d = 0.5U$. These plots show more clearly the narrowing of the co-existence region, corresponding to the green area in Figs. 3(a) and (c), and the red region in Figs. 3(b) and (d), as the system is moved away from the PHS point.

3.3. Signatures of the MIT in the charge density

An important point regarding the phase diagrams away from the PHS is that different phases in the system can be characterized not only by the zero-frequency spectral density $\rho(0)$ but also by the *charge density* n since the insulating region is characterized by half-filling, namely, $n = 1$. As such, the T versus U phase diagrams can be plotted by looking at n alone. In an analogy with $\rho_{\rm avg}(0)$ and $\Delta\rho(0)$ defined in Eq. (5), it is useful to define the following quantities related to the charge density:

$$n_{\rm avg} \equiv \left(n_{\rm M\to I} + n_{\rm I\to M}\right)/2\,, \qquad (6)$$
$$\Delta n \equiv |n_{\rm I\to M} - n_{\rm M\to I}|\,,$$

where $n_{\rm M\to I}$ and $n_{\rm I\to M}$ are calculated in the M → I and I → M paths respectively.

This one-to-one correspondence between the two quantities is evident in Figs. 4(a) and (b), which present similar $U \times T$ phase diagrams obtained from $\rho_{\rm avg}(0)$ and $n_{\rm avg}$, respectively, for $e_d = 0.45U$. Consequently, the phase diagrams of the system can also be effectively depicted by utilizing $n_{\rm avg}$. These are displayed in Figs. 5 (a) to (d), which show $n_{\rm avg}(\epsilon_d, U)$ and $\Delta n(\epsilon_d, U)$ for $T = 0.002$, see Figs. 5(a,b), and $T = 0.004$, see Figs. 5(c,d).

The goal here is to emphasize that the density n, an experimentally accessible quantity, can be used to effectively characterize the MIT transition away from the PHS point. Of course, this does not hold at

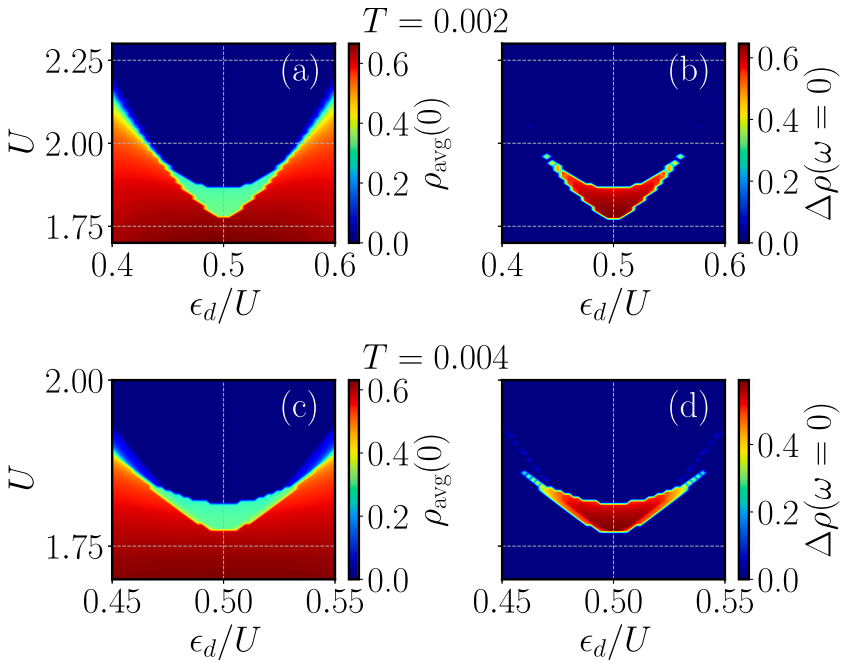

Fig. 3. DMFT-NCA phase diagram $U \times \epsilon_d$ of the Hubbard model for $T = 0.002$ (a,b) and $T = 0.004$ (c,d). Panels (a,c) show $\rho_{\text{avg}}(0)$ while panels (b,d) shows $\Delta\rho(0)$.

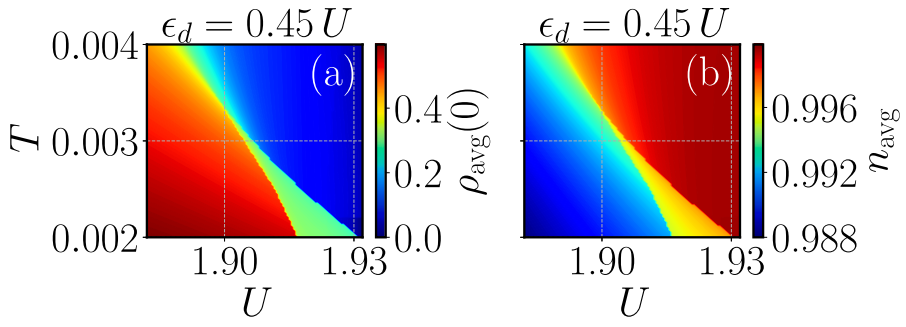

Fig. 4. DMFT-NCA phase diagram $U \times T$ for the Hubbard model away from particle-hole symmetry ($\epsilon_d = 0.45U$). Panel (a) shows the average $\rho_{\text{avg}}(0)$, while panel (b) shows the average density n_{avg}, which is remarkably similar.

the PHS point ($\epsilon_d = 0.5U$), since the system is always at half-filling ($n = 1$) independently of the phase.

4. Summary and conclusions

In this work, we have revisited the Mott metal–insulator transition (MIT) within the framework of the particle-hole asymmetric (PHA) Hubbard model on the Bethe lattice. For a temperature below a critical value, a phase transition takes place for two values of interaction, U_{c_1} and U_{c_2}, with a coexistence region between the latter. Above a critical temperature there is a crossover between the metal and insulator phases. However, for the asymmetric model we found a first-order transition only for U_{c_1}. For U_{c_2} we found a crossover between the two solutions with a pattern almost independent on the temperature.

Our results show that, in contrast with the well-studied particle-hole symmetric case, the PHA model exhibits a notably complex $U \times T$ phase diagram showing reduced value of the critical temperature T_c as well as a narrower co-existence region between metallic and insulating phases at low temperature. This is illustrated in the $U \times T$ and $U \times \epsilon_d$ phase diagrams, indicating the "shrinking" co-existence region with increasing temperature and/or breaking the particle-hole symmetry. The plots indicate that the transition between metallic and insulating phases is better defined when the system is away from PHS.

Away from the particle-hole symmetric point, the MIT is characterized by a co-existence region where the system exhibits both metallic and insulating properties over a range of interaction strengths U. This region, marked by "hysteresis loops" in the density and spectral density plots, becomes more pronounced at lower temperatures and is strongly influenced by the departure from PHS. This suggests that the first-order transition line is more sharply defined in the asymmetric model, offering clearer distinctions between the two phases.

Moreover, a key contribution of our work is the identification of the charge density n as a robust marker for the MIT transition in systems where particle-hole symmetry is broken since the transition will be marked by $n \to 1$. We notice that this behavior should occur in realistic material systems where PHS is broken by an asymmetric density of states, which can be schematically modeled, for instance, by a Bethe lattice incorporating second-neighbor hopping [56]. Unlike traditional approaches that rely on the zero-frequency spectral density, the charge density provides a more accessible and potentially experimentally verifiable parameter, especially in high-temperature regimes.

In summary, our study highlights the significant impact of breaking particle-hole symmetry on the MIT in the Hubbard model at finite

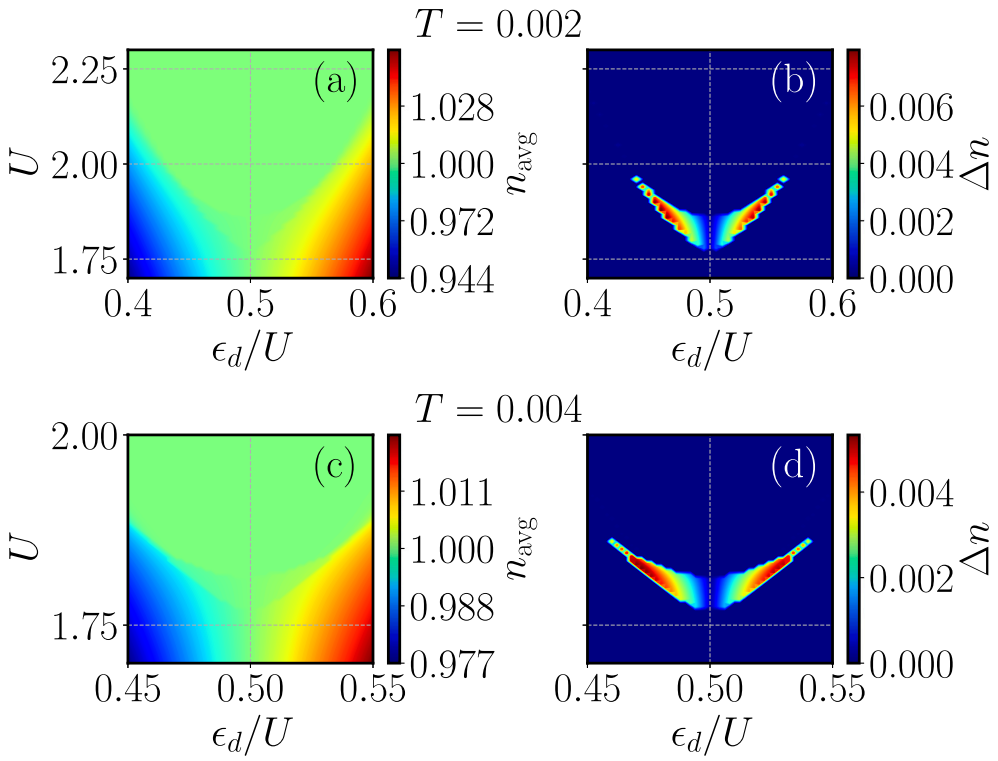

Fig. 5. Phase diagram $U \times \epsilon_d$ for the Hubbard model for $T = 0.002$ (a, b) and $T = 0.004$ (c, d). Panels (a, c) show n_{avg} while panels (b, d) shows Δn.

temperatures. The results underscore the need to consider symmetry effects in theoretical predictions and experimental observations of phase transitions in strongly correlated electron systems.

CRediT authorship contribution statement

Mateus Marques: Validation, Software, Data curation. **Bruno M. de Souza Melo:** Visualization, Validation, Software, Investigation. **Alexandre R. Rocha:** Writing – review & editing, Writing – original draft, Supervision, Methodology, Funding acquisition, Conceptualization. **Caio Lewenkopf:** Writing – review & editing, Writing – original draft, Supervision, Methodology, Investigation, Conceptualization. **Luis G.G.V. Dias da Silva:** Writing – review & editing, Writing – original draft, Supervision, Methodology, Investigation, Funding acquisition, Formal analysis, Conceptualization.

Declaration of competing interest

The authors declare that they have no known competing financial interests or personal relationships that could have appeared to influence the work reported in this paper.

Acknowledgments

The authors thank Maria Carolina Aguiar, Eduardo Miranda and Veronica Vildosola for the extremely helpful discussions and exchange of ideas. This work was supported by the Brazilian funding agencies CNPq (Grant Nos. 308351/2017-7, 423137/2018-2, 309789/2020-6, 313059/2020-9, and 312622/2023-6), FAPERJ (Grant E-26/202.882/2018), FAPESP (Grant Nos. 2017/02317-2, and 2022/15453-0) and CAPES/INCT (Grant Nos. 88887.169785/2018-00, 421701/2017-0).

Data availability

Data will be made available on request.

References

[1] Robert Peters, Thomas Pruschke, Half-filled hubbard model on a bethe lattice with next-nearest-neighbor hopping, Phys. Rev. B 79 (4) (2009) 045108.
[2] Kristjan Haule, Chuck Hou Yee, Kyoo Kim, Dynamical mean-field theory within the full-potential methods: Electronic structure of $CeIrIn_5$, $CeCoIn_5$, and $CeRhIn_5$, Phys. Rev. B 81 (19) (2010) 195107.
[3] Sangkook Choi, Andrey Kutepov, Kristjan Haule, Mark van Schilfgaarde, Gabriel Kotliar, First-principles treatment of mott insulators: linearized QSGW+DMFT approach, Npj Quantum Mater. 1 (1) (2016) 16001.
[4] Andreas Rüegg, Hsiang Hsuan Hung, Emanuel Gull, Gregory A. Fiete, Comparative DMFT study of the e_g-orbital Hubbard model in thin films, Phys. Rev. B 89 (8) (2014) 085122.
[5] You Zhou, Shriram Ramanathan, Correlated electron materials and field effect transistors for logic: A review, Crit. Rev. Solid State Mater. Sci. 38 (4) (2013) 286–317.
[6] Rok Žitko, Convergence acceleration and stabilization of dynamical mean-field theory calculations, Phys. Rev. B 80 (12) (2009) 125125.
[7] N.F. Mott, Metal–insulator transition, Rev. Modern Phys. 40 (4) (1968) 677–683.
[8] Henrik Kajueter, Gabriel Kotliar, Goetz Moeller, Doped Mott insulator: Results from mean-field theory, Phys. Rev. B 53 (24) (1996) 16214–16226.
[9] Sharareh Sayyad, Rok Žitko, Hugo U.R. Strand, Philipp Werner, Denis Golež, Comparative study of nonequilibrium insulator-to-metal transitions in electron–phonon systems, Phys. Rev. B 99 (4) (2019) 045118.
[10] R. Qiu, E. Bousquet, A. Cano, Pressure-induced insulator–metal transition in $EuMnO_3$, J. Phys.: Condens. Matter. 29 (30) (2017) 305801.
[11] M.J. Rozenberg, G. Kotliar, X.Y. Zhang, Mott-hubbard transition in infinite dimensions II, Phys. Rev. B 49 (15) (1994) 10181–10193.
[12] J. Hubbard, Electron Correlations in Narrow Energy Bands, Proc. R. Soc. Lond. A 276 (1365) (1963) 238–257.
[13] J. Hubbard, Electron correlations in narrow energy bands. II. The degenerate band case, Proc. R. Soc. Lond. A 277 (1369) (1964) 237–259.
[14] G. Kotliar, Sahana Murthy, M.J. Rozenberg, Compressibility Divergence and the Finite Temperature Mott Transition, Phys. Rev. Lett. 89 (4) (2002) 046401.
[15] A. Georges, G. Kotliar, W. Krauth, M. Rozenberg, Dynamical mean-field theory of strongly correlated fermion systems and the limit of infinite dimensions, Rev. Modern Phys. 68 (1) (1996) 13–125.
[16] K. Held, Electronic structure calculations using dynamical mean field theory, Adv. Phys. 56 (6) (2007) 829–926.
[17] V. Vildosola, L.V. Pourovskii, L.O. Manuel, P. Roura-Bas, Reliability of the one-crossing approximation in describing the mott transition, J. Phys.: Condens. Matter. 27 (48) (2015) 485602.

[18] R. Bulla, D. Vollhardt, T.A. Costi, Finite-temperature numerical renormalization group study of the Mott transition, Phys. Rev. B 64 (4) (2001) 045103.
[19] Jaewook Joo, Viktor Oudovenko, Quantum Monte Carlo calculation of the finite temperature Mott-Hubbard transition, Phys. Rev. B 64 (19) (2001) 193102.
[20] Martin Eckstein, Philipp Werner, Nonequilibrium dynamical mean-field calculations based on the noncrossing approximation and its generalizations, Phys. Rev. B 82 (11) (2010) 115115.
[21] Th. Pruschke, D.L. Cox, M. Jarrell, Hubbard model at infinite dimensions: Thermodynamic and transport properties, Phys. Rev. B 47 (7) (1993) 3553–3565.
[22] Ning Hua Tong, Shun Qing Shen, Fu Cho Pu, Mott-Hubbard transition in infinite dimensions, Phys. Rev. B 64 (23) (2001) 235109.
[23] H. Terletska, J. Vučičević, D. Tanasković, V. Dobrosavljević, Quantum critical transport near the mott transition, Phys. Rev. Lett. 107 (2011) 026401.
[24] Vladimir. Dobrosavljevic, Nandini. Trivedi, James M. Valles Jr., Conductor-Insulator Quantum Phase Transitions, vol. 06, Oxford University Press, 2012.
[25] D.O. Demchenko, A.V. Joura, J.K. Freericks, Effect of particle-hole asymmetry on the Mott-Hubbard metal–insulator transition, Phys. Rev. Lett. 92 (21) (2004) 216401.
[26] Martin Eckstein, Marcus Kollar, Michael Potthoff, Dieter Vollhardt, Phase separation in the particle-hole asymmetric Hubbard model, Phys. Rev. B 75 (12) (2007) 125103.
[27] D.J. García, E. Miranda, K. Hallberg, M.J. Rozenberg, Mott transition in the Hubbard model away from particle-hole symmetry, Phys. Rev. B 75 (2007) 121102.
[28] Daniel S. Fisher, G. Kotliar, G. Moeller, Midgap states in doped mott insulators in infinite dimensions, Phys. Rev. B 52 (24) (1995) 17112–17118.
[29] Philipp Werner, Andrew J. Millis, Doping-driven Mott transition in the one-band Hubbard model, Phys. Rev. B 75 (8) (2007) 085108.
[30] David E. Logan, Martin R. Galpin, Mott insulators and the doping induced mott transition within DMFT: exact results for the one-band hubbard model, J. Phys.: Condens. Matter. 28 (2) (2015) 025601.
[31] J. Vucicevic, D. Tanaskovic, M.J. Rozenberg, V. Dobrosavljevic, Bad-metal behavior reveals Mott quantum criticality in doped hubbard models, Phys. Rev. Lett. 114 (2015) 246402.
[32] M.C.O. Aguiar, V. Dobrosavljević, E. Abrahams, G. Kotliar, Scaling behavior of an anderson impurity close to the mott-anderson transition, Phys. Rev. B 73 (2006) 115117.
[33] Helena Braganç M.C.O, Vučičević J. Aguiar, D. Tanasković, V. Dobrosavljević, Anderson localization effects near the mott metal–insulator transition, Phys. Rev. B 92 (2015) 125143.
[34] P.W. Anderson, Localized magnetic states in metals, Phys. Rev. 124 (1) (1961) 41–53.
[35] G. Kotliar, S.Y. Savrasov, K. Haule, V.S. Oudovenko, O. Parcollet, C.A. Marianetti, Electronic structure calculations with dynamical mean-field theory, Rev. Modern Phys. 78 (3) (2006) 865–951.
[36] Eleftherios N. Economou, Green's Functions in Quantum Physics, third ed., Springer, 2006.
[37] Kei Yosida, Kosaku Yamada, Perturbation Expansion for the Anderson Hamiltonian, Prog. Theor. Phys. Sup. 46 (46) (1970) 244–255.
[38] Kei Yosida, Kosaku Yamada, Perturbation expansion for the Anderson Hamiltonian. III, Progr. Theoret. Phys. 53 (5) (1975) 1286–1301.
[39] Kosaku Yamada, Perturbation expansion for the Anderson Hamiltonian. II, Progr. Theoret. Phys. 53 (4) (1975) 970–986.
[40] Kenneth G. Wilson, The renormalization group: Critical phenomena and the kondo problem, Rev. Modern Phys. 47 (4) (1975) 773–840.
[41] R. Bulla, Zero temperature metal–insulator transition in the infinite-dimensional Hubbard model, Phys. Rev. Lett. 83 (1) (1999) 136–139.
[42] Alba Theumann, Self-consistent solution of the Anderson model, Phys. Rev. 178 (1969) 978–984.
[43] C. Lacroix, Density of states for the Anderson model, J. Phys. F: Met. Phys. 11 (11) (1981) 2389–2397.
[44] C. Lacroix, Density of states for the asymmetric Anderson model, J. Appl. Phys. 53 (3) (1982) 2131–2133.
[45] Yigal Meir, Ned S. Wingreen, Patrick A. Lee, Transport through a strongly interacting electron system: Theory of periodic conductance oscillations, Phys. Rev. Lett. 66 (23) (1991) 3048–3051.
[46] Vyacheslavs Kashcheyevs, Amnon Aharony, Ora Entin-Wohlman, Applicability of the equations-of-motion technique for quantum dots, Phys. Rev. B 73 (12) (2006) 125338.
[47] Raphaël Van Roermund, Shiue-yuan Shiau, Mireille Lavagna, Anderson model out of equilibrium: Decoherence effects in transport through a quantum dot, Phys. Rev. B 81 (2010) 165115.
[48] Mireille Lavagna, Transport through an interacting quantum dot driven out-of-equilibrium, J. Phys.: Conf. Ser. 592 (2015) 012141.
[49] Piers Coleman, New approach to the mixed-valence problem, Phys. Rev. B 29 (6) (1984) 3035–3044.
[50] N.E. Bickers, Review of techniques in the large-N expansion for dilute magnetic alloys, Rev. Modern Phys. 59 (4) (1987) 845–939.
[51] Th. Pruschke, N. Grewe, The Anderson model with finite Coulomb repulsion, Z. Phys. B 74 (4) (1989) 439–449.
[52] J.E. Hirsch, R.M. Fye, Monte Carlo Method for Magnetic Impurities in Metals, Phys. Rev. Lett. 56 (23) (1986) 2521–2524.
[53] B.M. de Souza Melo, L.G.G.V. Dias da Silva, A.R. Rocha, C. Lewenkopf, Quantitative comparison of Anderson impurity solvers applied to transport in quantum dots, J. Phys.: Condens. Matter. 32 (9) (2020) 095602.
[54] C.N. Sposetti, L.O. Manuel, P. Roura-Bas, Qualitative breakdown of the noncrossing approximation for the symmetric one-channel Anderson impurity model at all temperatures, Phys. Rev. B 94 (8) (2016) 085139.
[55] Norbert Grewe, Sebastian Schmitt, Torben Jabben, Frithjof B. Anders, Conserving approximations in direct perturbation theory: new semianalytical impurity solvers and their application to general lattice problems, J. Phys.: Condens. Matter. 20 (36) (2008) 365217.
[56] Martin Eckstein, Marcus Kollar, Krzysztof Byczuk, Dieter Vollhardt, Hopping on the Bethe lattice: Exact results for densities of states and dynamical mean-field theory, Phys. Rev. B 71 (23) (2005) 1–13.